The Centromeric/Nucleolar Chromatin Protein ZFP-37 May Function to Specify Neuronal Nuclear Domains*

Emmanuel Payen‡§, Ton Verkerk‡, Dave Michalovich‡¶, Sandra D. Dreyer‖, Andreas Winterpacht‖, Brendan Lee, Chris I. De Zeeuw‡‡§§, Frank Grosveld‡, and Niels Galjart‡¶¶**

*From the ‡Department of Cell Biology and Genetics and the ‡‡Department of Anatomy, Erasmus University, P. O. Box 1738, 3000 DR Rotterdam, The Netherlands, the **Department of Molecular and Human Genetics, Baylor College of Medicine, Houston, Texas 77030, and ‖Children's Hospital, University of Mainz, D-55101 Mainz, Germany*

Murine ZFP-37 is a member of the large family of C_2H_2 type zinc finger proteins. It is characterized by a truncated NH_2-terminal Krüppel-associated box and is thought to play a role in transcriptional regulation. During development *Zfp-37* mRNA is most abundant in the developing central nervous system, and in the adult mouse expression is restricted largely to testis and brain. Here we show that at the protein level ZFP-37 is detected readily in neurons of the adult central nervous system but hardly in testis. In brain ZFP-37 is associated with nucleoli and appears to contact heterochromatin. Mouse and human ZFP-37 have a basic histone H1-like linker domain, located between KRAB and zinc finger regions, which binds double-stranded DNA. Thus we suggest that ZFP-37 is a structural protein of the neuronal nucleus which plays a role in the maintenance of specialized chromatin domains.

It was proposed recently that the large family of nucleic acid-binding C_2H_2 type zinc finger genes is divided into two classes (1). One consists of zinc finger genes that encode small protein families with evolutionary conserved finger clusters of three to five units. These proteins bind to similar DNA sequences and play an important role either as housekeeping proteins or as regulatory factors during development. Examples of this class of zinc finger genes are *Gli-1*, *Krox-20*, *WT1*, *Egr-1*, and *Sp1*. The second class consists of C_2H_2 zinc finger genes, which often contain more than 10 zinc finger units/gene. Because some of these genes are not well conserved among species it was speculated that they must have arisen late in evolution. For example *ZNF91*, which encodes a protein with 35 zinc fingers, is found duplicated many times in man and primates, but the gene cluster is undetectable in rodents (2).

The function of the protein products encoded by this class of genes could be to bind to repetitive DNA sequences (1).

Common structural motifs other than the zinc finger characterize the second class of genes. These include the finger-associated box (FAX; Ref. 3), finger-associated repeats (FAR; Ref. 4), and Krüppel-associated box (KRAB)[1] domains (5). The KRAB region is almost always found at the NH_2 terminus of Krüppel-like zinc finger proteins (ZFPs). The KRAB domain is estimated to be present in about one-third of all C_2H_2 type zinc fingers (5) but has also been found in two non-zinc finger genes (6). It has been subdivided into a conserved A region and a more degenerate B domain, which are often encoded by two different exons. Accumulating evidence supports a function for the KRAB domain in transcriptional repression (7–10). Because of this the KRAB ZFPs are generally assumed to be DNA-binding transcriptional regulators.

We are interested in neuronal nuclear architecture and are investigating the molecular mechanisms that underlie the adaptations in gene expression and protein synthesis patterns allowing these postmitotic cells to function in complex neuronal circuitries. The murine *Zfp-37* gene encodes a protein that potentially plays a role in these processes. It was described originally as a gene transcribed exclusively in testis and encoding a protein with 12 zinc fingers at its COOH terminus (11, 12). We then showed that it is a member of the KRAB zinc finger gene family and that it is not only expressed in testis but also in the developing and adult central nervous system and, at lower levels, in a number of other tissues (13). In adult brain, the *Zfp-37* message is specific to neurons, with regional differences in expression levels found throughout the brain. Multiple protein isoforms of the *Zfp-37* gene can be generated through the use of different promoters and alternative splicing of pre-mRNAs. The major isoforms have a predicted molecular mass of 67 kDa, and they contain a truncated KRAB-A and a complete KRAB-B region. The minor form is 62 kDa and lacks the truncated KRAB-A region. By virtue of sequence elements located in its 3′-untranslated region *Zfp-37* was predicted to be an immediate-early response gene (13). This combination of highly regulated expression in neurons of a potential immediate-early transcription factor provided the basis for a further analysis of the role of *Zfp-37*.

Here we show that ZFP-37 isoforms of ~67 kDa are ex-

[1] The abbreviations used are: KRAB, Krüppel-associated box; ZFP, zinc finger protein; GST, glutathione *S*-transferase; PCR, polymerase chain reaction; bp, base pair(s); GFP, green fluorescent protein; BFP, blue fluorescent protein; NoLS, nucleolus-localizing sequence; FITC, fluorescein isothiocyanate; DAPI, 4′,6-diamidino-2-phenylindole; DABCO, 1,4-diazabicyclo-[2,2,2]octane.

pressed *in vivo* and that they contain the truncated KRAB-A region, indicating that the protein might function as a transcriptional repressor. ZFP-37 is detected in neurons of the adult central nervous system but hardly in testis. In the brain ZFP-37 localizes to constitutive heterochromatin attached to nucleoli, and/or it decorates the interior of the nucleolus. Furthermore, both mouse and human ZFP-37 contain a DNA binding domain that is located in the basic amino acid stretch between KRAB and zinc finger regions. This domain has a preference for double-stranded DNA, and it resembles the basic COOH-terminal DNA binding motif of histone H1. Together, these data suggest that ZFP-37 is involved in the functional specialization of neuronal nuclear domains.

<center>EXPERIMENTAL PROCEDURES</center>

Bacterial Fusion Proteins—Mouse brain-derived *Zfp-37* cDNA (13) was digested with restriction enzymes to give DNA fragments suitable for subcloning into the bacterial expression plasmids pGEX2T and pGEX3X (Pharmacia). The following constructs were generated initially: GST-ZFP-37 (containing nucleotides 148–1870 of the mouse *Zfp-37* cDNA sequence), GST-K(RAB)A (containing nucleotides 148–210), GST-KL1 (containing nucleotides 148–555), GST-3ZF (containing nucleotides 1550–1870), and GST-8ZF (containing nucleotides 1160–1870; see also Fig. 2*A*). Subsequent constructs (see Fig. 4*A*) were generated by PCR using *Zfp-37*-specific primers with anchored restriction enzyme sites. The linker regions of rKr2 (U27186), RNU67082, mouse kid-1 (L77247), NK10 (X79828), and ZFP60 (U48721) were taken from the data base and primers designed for reverse transcriptase-PCR which yielded the complete linker region in between KRAB and zinc finger domains. The hL1 fusion protein was also obtained by PCR, using a human *Zfp-37* cDNA clone as template.[2] PCR fragments were subcloned into pGEX, and clones were verified by sequence analysis. Bacterial fusion proteins were induced and purified as described (15). Except for GST-ZFP-37, all fusion proteins were made in large quantities.

DNA Binding Analyses—DNA fragments for bandshift assays were isolated using standard procedures (16). The 140-bp probe used in most bandshift experiments contains 106 bp from intron 3 of the *Zfp-37* gene. This fragment was PCR amplified and cloned into the *Eco*RV site of Bluescript (Stratagene). A 140-bp fragment used for bandshift analysis was generated by excision with *Eco*RI and *Sal*I. Radioactive probes for the Southwestern analysis were made as described (17).

Southwestern assays were performed as published previously (18). For bandshift experiments, GST fusion proteins were purified with the use of glutathione beads (Pharmacia). Before bandshift assays proteins were diluted to the required concentration in binding buffer (5 mM Tris (pH 8.0), 0.5 mM dithiothreitol, 0.5 mM EDTA, 25 mM NaCl, 1% Ficoll), occasionally in the presence of 1 mg/ml bovine serum albumin. Various concentrations of fusion protein were mixed with 2–10 ng of probe in binding buffer and incubated for 20 min. When required, cold competitor DNA was added simultaneously to the samples. Protein-DNA complexes were resolved on 4% acrylamide gels. After electrophoresis, the gels were dried and exposed to PhosphorImager screens (Molecular Dynamics).

Affinity coelectrophoresis was carried out as described previously (19, 20). Increasing concentrations of the Pwt peptide were used for this analysis, together with 0.5 ng of the 140-bp DNA probe. Gel electrophoresis was carried out in 1% low melting agarose gels in Tris acetate buffer containing 50 mM NaCl. Gels were dried after electrophoresis and exposed to PhosphorImager screens.

Peptide Synthesis and Antibody Production—Peptides were synthesized according to the solid phase method (21). The sequences of Pwt, Pshort, and Pmut peptides are shown in Fig. 4*B*. In addition we made a Pwt peptide with an extra cysteine residue at its NH$_2$ terminus. 2 mg of this sulfhydryl-containing peptide was conjugated to 2 mg of maleimide-activated bovine serum albumin using the Imject activated immunogen conjugation kit (Pierce).

Purified bacterial fusion proteins or conjugated peptide preparations were injected into rabbits, in a suspension containing Freund's incomplete adjuvant (Difco). After three boosts with the respective antigens, antibodies were obtained and tested on Western blots containing COS-1 cell extracts. Antibodies were purified using protein A-Sepharose (Pharmacia) and, if needed, subsequently affinity purified on filter

strips containing the various bacterial fusion proteins. MeCP2 antibodies (22) and histone H1 antibodies (23) were kind gifts of Drs. A. Bird and M. Parseghian, respectively.

Western Blot Analysis—Nuclear extracts from embryonic and adult mouse tissues were made as published (24) and protein concentrations measured using the BCA assay (Pierce). Total protein extracts from COS-1 cells or tissues were made by freeze-thawing and sonication of cell suspensions followed by boiling in SDS sample buffer containing dithiothreitol. About 25–50 μg of (nuclear) protein lysate was loaded per lane on SDS-polyacrylamide gels (16). After electrophoresis, proteins were blotted, and filters were blocked for 16 h in 50 mM Tris (pH 8.0), 150 mM NaCl (Tris-buffered saline), and 0.05% (v/v) Tween 20 (Sigma), containing 3% (w/v) bovine serum albumin (Sigma). Antibody incubations were done for 2–16 h, in the same buffer. Antibody-antigen interactions were detected according to standard procedures (16).

Immunofluorescence Studies—For ZFP-37 overexpression studies, two constructs, encoding different isoforms of mouse ZFP-37, were subcloned into a derivative of the mammalian expression vector pCD-X (25). In one clone a genomic fragment was linked to the full-length *Zfp-37* cDNA sequence to enable translation initiation from the first methionine in the mouse cDNA sequence (13). The second construct encompassed nucleotides 145–2377 of the *Zfp-37* cDNA (13), to allow only translation initiation from the second methionine in the mouse cDNA.

To verify the localization of overexpressed ZFP-37, the protein was fused to a modified form of green fluorescent protein (26, 27), called hGFP-S65T (CLONTECH). hGFP-S65T was further mutagenized at 3 amino acid residues (T65S, Y66H, Y145F) with the transformer site-directed mutagenesis kit (CLONTECH) to yield blue fluorescent protein, or BFP (28). A cDNA subclone of human ribosomal protein S6 (29), which encodes a nucleolus-localizing sequence (NoLS), was then linked in-frame to BFP.

COS-1 cells (30) were transfected as described previously (31). After 24 h cells were fixed using 3% paraformaldehyde in phosphate-buffered saline and permeabilized with 0.05% Triton X-100 in phosphate-buffered saline. Cells were incubated subsequently with affinity-purified anti-ZFP-37 antibodies followed by a detection step with FITC-labeled goat anti-rabbit antibody (Nordic Immunological Laboratories, Tilburg, The Netherlands). All antibodies gave similar results in these experiments, except the one against GST-KRAB-A, which did detect COS-1 cell-derived ZFP-37, produced from the first methionine, but not ZFP-37 produced from the second methionine (data not shown). The ZFP-37-GFP and NoLS-BFP proteins were detected in live transfected COS-1 cells using an Olympus IX-70 inverted microscope with appropriate filterblocks (Chromacorp). Images were captured with a Sony 3CCD color video camera and digital still recorder.

For the detection of ZFP-37 in mouse tissues, wild type or transgenic mice were anesthetized using 50 μl of Hypnodil (Janssen Pharmaceutica) and perfused transcardially with 50 ml of saline solution followed by 50 ml of freshly prepared 4% (w/v) paraformaldehyde in phosphate-buffered saline. Tissues were removed after perfusion and postfixed in the same solution for 1–2 h at 4 °C. Tissues were embedded in paraffin (Merck 1.07157), and 10-μm sections were cut on a microtome. Sections were spread onto Mentzel Superfrost slides and dried. Paraffin was removed using xylene, and sections were rehydrated through an ethanol series. Subsequently, slides were immersed into 10 mM sodium citrate buffer (pH 6.0), microwave treated (3 × 5 min at 600 watts with a 5-min rest period in between), and cooled down slowly in the same buffer. Sections were then rinsed with 10 mM Tris (pH 7.6), 50 mM NaCl (TN buffer), followed by three washes with the same buffer containing 0.05% (v/v) Tween 20 (TNT buffer). Blocking of nonspecific sites was carried out for 2–3 h at room temperature using 3% bovine serum albumin in TNT buffer. Antibody incubations were done overnight at 4 °C in the same buffer. Sections were then washed in TNT buffer and incubated with FITC-labeled secondary antibody. After further washing, sections were dried and mounted with DAPI/DABCO/glycerol medium.

<center>RESULTS</center>

ZFP-37 Contains a Histone H1-like DNA Binding Domain—Recently the gene encoding the human counterpart of ZFP-37 was isolated and characterized. Comparison of the protein product with murine ZFP-37 reveals that these proteins are almost identical in their zinc finger domains (Fig. 1*A*). Therefore, the molecular partners of this region could be conserved between mouse and man. Upstream of the zinc finger region

---

[2] S. Dreyer, A. Winterpacht, and B. Lee, unpublished results.
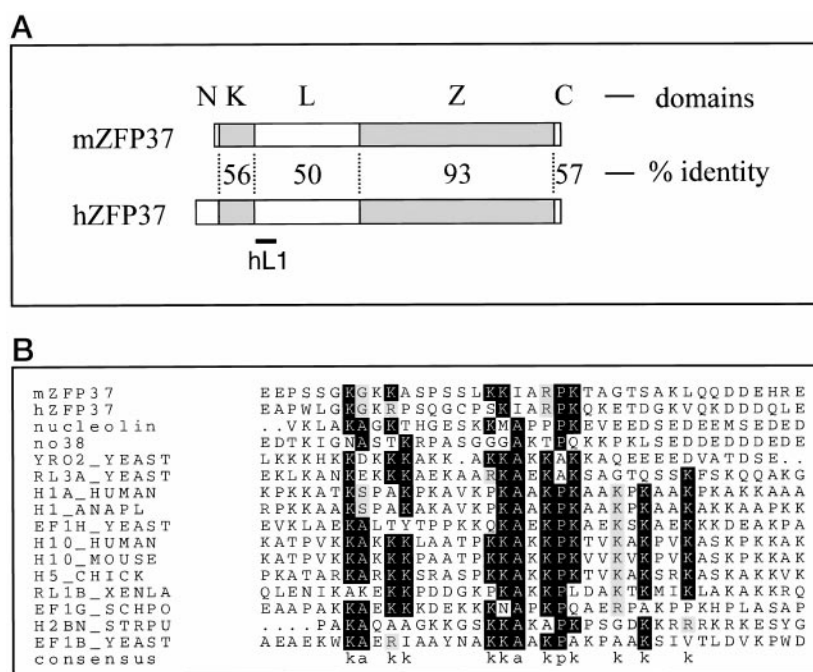[2] S. Dreyer, A. Winterpacht, and B. Lee, unpublished results.

FIG. 1. **Structure of mouse and human ZFP-37 and alignment of their histone H1-like domains.** *Panel A*, ZFP-37 structure. Mouse and human ZFP-37 can be divided into five domains: 1) an NH_2-terminal region (*N*), which is longer in the human protein; 2) a truncated KRAB domain (*K*; *hatched bar*); in both proteins this domain lacks 17 amino acids that were shown to be important for *in vitro* repression activity in other KRAB domains; 3) a basic linker region between KRAB and zinc finger domains (*L*); 4) the zinc finger region (*Z*; *hatched bar*); and 5) a short and highly acidic COOH-terminal region (*C*). The similarity among the different regions is indicated. hL1 is the part of human ZFP-37 which was fused to GST for DNA binding studies (see Figs. 2 and 4). This short region does contain the histone H1-like domain described below. *Panel B*, comparison of the linker regions of mouse and human ZFP-37 with the Swissprot data base, using BlastP, reveals the presence of a histone H1-like domain in ZFP-37. Several proteins with a similar region were selected from this comparison and aligned to the linker region of ZFP-37 using Pileup (Wisconsin package 8.0, Genetics Computer Group, Madison, WI). Not all histone H1 sequences are included. Short protein regions of highest similarity were selected and run through Boxshade 3.21 (http://ulrec3.unil.ch:80). More than 50% identity is indicated with a *black box*; similar residues are indicated by a *gray box*.

the similarity between mouse and human proteins drops to ~50%. In addition, human ZFP-37 contains a longer NH_2-terminal region upstream of the KRAB domain. This raises the question of whether these less conserved regions serve the same function in mouse and man. However, alignment of the ZFP-37 linker, located between KRAB and zinc finger domains, to the Swissprot data base revealed the presence of a small basic region in both linkers, embedded in a framework of alanine and proline residues, which resembles the COOH-terminal tail of a number of histone H1 variants and other nuclear and nucleolar proteins (Fig. 1*B*). Domains of this kind may bind to the minor groove of DNA in a nonspecific manner (for review, see Ref. 32). Thus, the structure of both murine and human ZFP-37 predicts the presence of two nucleic acid binding motifs: a highly conserved zinc finger region located at the COOH terminus of both proteins and a histone H1-like region located between the zinc finger and KRAB domains.

DNA Binding Properties of ZFP-37—Binding site selection experiments have been developed to identify high affinity DNA binding sites for transcription factors (33). This protocol has also been applied successfully in the case of multi-zinc finger proteins of the C_2H_2 type (*e.g.* Ref. 34). To identify ZFP-37-responsive sequence(s) using this approach, bacterial fusion proteins were made, containing either full-length ZFP-37 or truncated parts of the protein, linked to GST. Initially, five different fusion proteins were made (Fig. 2*A*, *upper panel*), all of which are soluble (data not shown). Except for the full-length ZFP-37-GST fusion protein, each polypeptide was produced in large quantities and could be purified as a single species using affinity chromatography (data not shown). However, none of the five proteins yielded a specific DNA binding site when tested with the selection protocol (data not shown). The DNA binding capacities of the histone H1-like domain and zinc finger region were therefore investigated in a Southwestern blot assay (Fig. 2*A*). Bacterial proteins were allowed to renature on a blot in the presence or absence of zinc and incubated with different radioactively labeled DNA fragments. This analysis demonstrates that the zinc finger region of ZFP-37 does have the capacity to bind DNA but only when the fingers have been allowed to renature in the presence of zinc (Fig. 2A, *lower left panel*). Because multiple probes were bound (data not shown) we conclude that in this assay the zinc fingers bind DNA nonspecifically. In accordance with our prediction, the fusion protein called KL1, which contains the histone H1-like domain described above, is also able to bind DNA, in both the presence and absence of zinc chelators, whereas GST or GST-KA does not bind (Fig. 2*A*, *lower left* and *right panels*). Thus ZFP-37 indeed harbors two different regions with the potential to bind DNA.

Conservation of the DNA binding activity of mouse ZFP-37 in the human protein would indicate that this is a physiologically relevant feature of ZFP-37. Hence the domain from human ZFP-37, encompassing the histone H1-like stretch (hL1, see Fig. 1*A*), was fused in-frame to GST and tested by Southwestern assay. In addition, we checked the linker regions from five other KRAB ZFPs for potential DNA binding capacity. These linkers were chosen because they are basic (*i.e.* kid-1 (35), rKr2 (36), and ZFP-60 (37)) or because they contain cysteine residues (*i.e.* NK10 (38) and RNU67082) and might have the potential to form a nucleic acid binding pocket. Each of the fusion proteins was produced in comparable quantity in bacteria, and these amounts were sufficient to be detected on blots stained with Amido Black (Fig. 2*B*, *lower panel*). However, when tested in the Southwestern assay, only hL1 bound DNA substantially
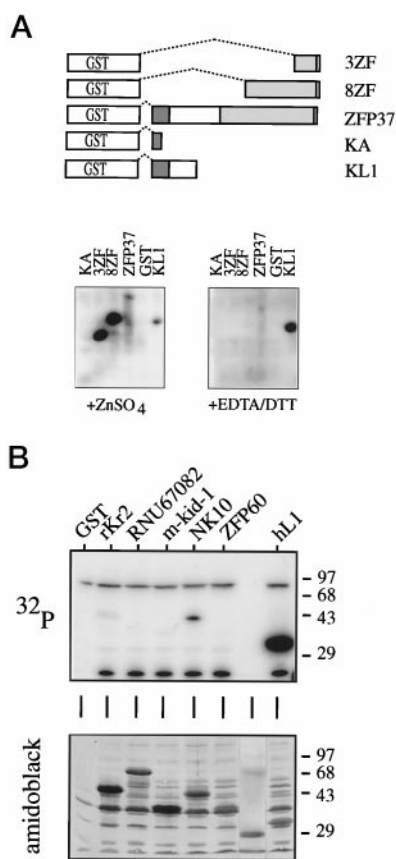
FIG. 2. **Southwestern analysis of DNA binding activity in ZFP-37 and other KRAB-ZFPs.** *Panel A*, GST was linked to different regions of ZFP-37, using restriction enzyme sites present in the mouse cDNA. The fusion proteins contain the last three zinc fingers (3ZF) or the last eight zinc fingers (8ZF) of ZFP-37; an almost complete protein (ZFP37); part of the KRAB-A domain of ZFP-37 (KA); or the KRAB domain with part of the linker region (KL1). The five fusion proteins plus a GST negative control were induced in bacteria, and protein lysates were separated by SDS-polyacrylamide gel electrophoresis and blotted. Proteins were allowed to renature, either in the presence of zinc (*lower left panel*) or with zinc chelators (*lower right panel*). Blots were probed with radioactively labeled *Zfp-37* cosmid DNA, washed, and exposed. *Panel B*, the linker domains of hL1 and five other KRAB-ZFPs were isolated and fused in-frame to GST. Proteins were induced in bacteria, and crude lysates were analyzed as in *panel A*, in the presence of zinc chelators (*upper panel*). Blots were stained with Amido Black after radioactive detection to estimate the quantity of the various GST fusion proteins (*lower panel*). The GST extract in the *left lane* is identical to that in *panel A*. It lacks the low molecular weight hybridizing band, present in the other extracts, because in *panel A*, aliquots of clear bacterial supernatants were put on gel, whereas in *panel B*, crude lysates were used. The *lane* between ZFP60 and hL1 contains marker proteins; sizes are indicated to the *right*. Expected sizes for the different GST-linker fusion proteins are: 44 kDa (rKr2), 59 kDa (RNU67082), 39 kDa (m-kid-1), 42 kDa (NK10), 38 (ZFP60), and 34 kDa (hL1). As shown in the *lower panel* there is a good correlation between the predicted and the observed molecular mass after SDS-polyacrylamide gel electrophoresis.

(Fig. 2*B*, *upper panel*). These data suggest that the DNA binding capacity of the mouse ZFP-37 linker region is indeed conserved in man and is unique to ZFP-37.

Fusion protein binding to DNA was characterized further in bandshift assays, using probes between 30 and 250 bp. Under the conditions tested GST-3ZF and GST-8ZF did not bind DNA (data not shown). It was not possible to investigate the complete zinc finger region because GST-ZFP-37 is very difficult to elute using glutathione beads and is never eluted as a single pure species. Although we subsequently synthesized other fusion proteins that lacked the KRAB and linker regions but

contained 10–12 zinc fingers, we found that these fusion proteins also are difficult to purify (data not shown). Hence the zinc finger domain was not analyzed further using the GST system. In contrast, GST-KL1, which is eluted in high yields and as a pure species, binds efficiently to all tested probes larger than 50 bp (data not shown). We next tested the influence of protein concentration on KL1-DNA complex formation using a probe of 140 bp (Fig. 3*A*). This showed that between 163 and 325 nM KL1, protein-DNA interactions become stable, *i.e.* complexes migrate as a single species through the acrylamide gel. The increase in apparent size of protein-DNA complexes at increasing protein concentrations suggests that more than one molecule of KL1 needs to be bound per DNA molecule to get a rigid structure that can migrate stably through a gel. This in turn indicates that KL1 binds DNA cooperatively. Probes smaller than 50 bp might not be able to accommodate enough protein molecules to ensure a stable interaction with DNA.

The specificity of DNA binding by the linker domain of ZFP-37 was investigated in more detail in competition bandshifts (Fig. 3*B*). Increasing amounts (10-, 50-, and 200-fold excess) of unlabeled single- and double-stranded DNA or RNA competitors were added to reactions that contained an excess of KL1 fusion protein complexed to 5 ng of the 140-bp probe. In these experiments the best competitor was sheared mouse genomic DNA, which is able to abolish probe-protein interactions completely when added at a 10-fold excess (Fig. 3*B*). Roughly 5-fold more of the other double-stranded nucleic acids (both DNA and RNA) is needed to compete away binding of the labeled probe to KL1, whereas single-stranded competitors and poly(dI·dC) are effective only at very high concentrations. Interestingly, the addition of denatured RNA to KL1-DNA complexes caused an apparent increase in the size of these complexes instead of a decrease (or disappearance) as in the other lanes. One explanation for this phenomenon is that this non-labeled competitor is able to attach to the KL1-DNA complexes. The competition by RNA is not caused by contaminating DNA in the preparation because RNase-treated RNA does not compete (data not shown). Together the data indicate that the linker region of ZFP-37 has more affinity for double-stranded than for single-stranded nucleic acids, and it has a preference for DNA over RNA.

Minimal DNA Binding Domain in ZFP-37—To investigate whether the histone H1-like region in ZFP-37 is responsible for DNA binding, we generated fusion proteins with increasingly smaller and/or different parts of the KL1 linker domain (Fig. 4*A*). All proteins were made in sufficient quantity and could be affinity purified in a single step (data not shown). These proteins (and GST-hL1 described above) were next tested for their ability to complex with DNA by the addition of increasing amounts of protein to a fixed quantity of probe and resolving protein-DNA complexes on gel as described above for KL1 (data not shown). The various fusion proteins are depicted in Fig. 4*A*, and their relative DNA binding capacity, as determined in the bandshift experiments, is shown next to the proteins. A representative bandshift, showing the result of an incubation of excess amount of each fusion protein with DNA, distinguishes the DNA-binding proteins from those that do not bind. These data first of all confirm that hL1 binds DNA with the same efficiency as does KL1. Thus, both human and mouse ZFP-37 contain a DNA binding linker domain. Second, two elements in the linker domain of murine ZFP-37 can bind DNA independently. The first element (B1B9) encompasses the histone H1-like domain, the second (B2B10) is downstream of it; it is also rich in basic residues but lacks the characteristic positioning of alanine and proline residues (Fig. 4*A*). The concentration at which B2B10 binding is detected is about 1 μM, whereas B1B9
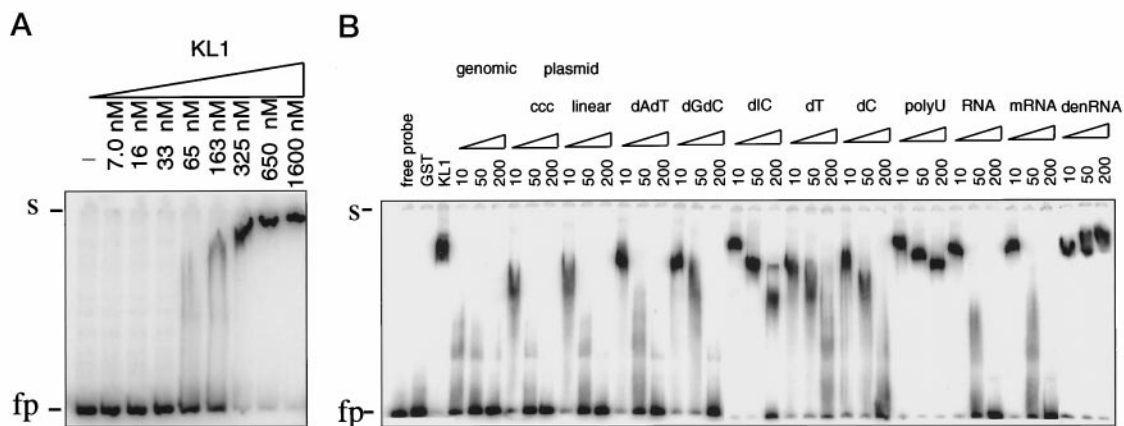
FIG. 3. **DNA binding characteristics of the linker domain of ZFP-37.** *Panel A*, to define the DNA binding properties of the linker domain of ZFP-37, purified GST-KL1 (abbreviated as KL1; see Fig. 2*A*) was incubated in increasing amounts with radioactive DNA. After incubation the protein-DNA complexes were separated from the free probe using an electrophoresis mobility shift assay. *S*, slot; *fp*, free probe. *Panel B*, KL1 fusion protein (2 μM) was incubated with 5 ng of a 140-bp DNA probe in the presence of 50, 250, or 1,000 ng (*i.e.* 10-, 50-, or 200-fold excess, respectively) of various competitors. Genomic DNA and RNA were extracted from mouse tail and liver, respectively. The controls, *i.e.* probe without fusion protein or incubated with GST or KL1, are shown in the *left three lanes*.
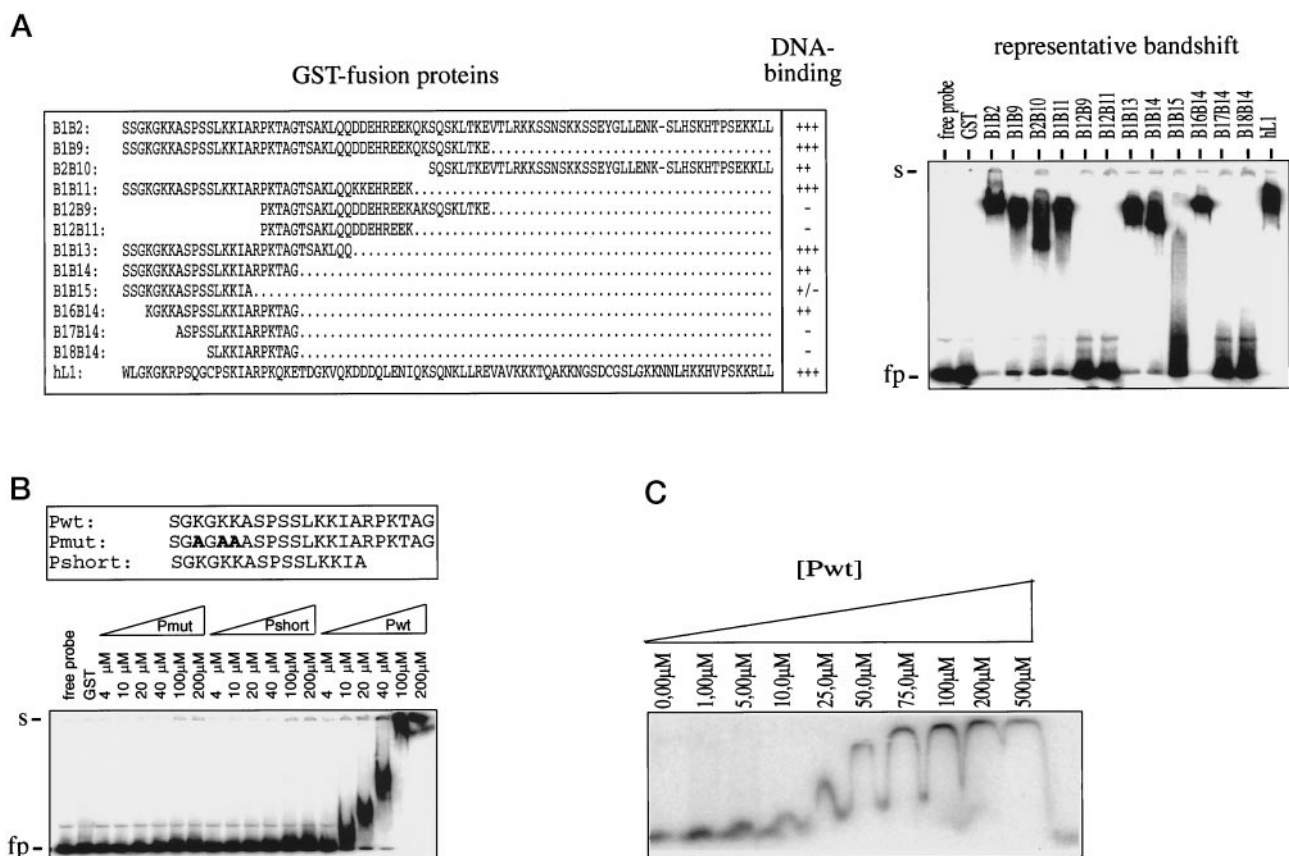

FIG. 4. **Minimal DNA binding domain in ZFP-37 linker.** *Panel A*, the linker region of mouse ZFP-37 was divided into increasingly smaller segments, and each fragment was cloned in-frame with GST, using PCR amplification with *Zfp-37*-specific primers (B1–B18). The amino acid sequences of the different linker fragments are shown in the *left panel*. The hL1 sequence is from the human ZFP-37 linker. The relative DNA binding strength of each fusion protein is given (+ + + indicates very strong binding; − indicates no binding); it was determined by electrophoresis mobility shift assay, similar to the experiment depicted in Fig. 3. A representative bandshift with a 3 μM concentration of each fusion protein and 5 ng of a 140-bp DNA probe is presented to the *right*. *S*, slot; *fp*, free probe. Control probe incubations without fusion protein and with GST only are shown in the *left two lanes*. *Panel B*, on the basis of the minimal core DNA binding region defined in *panel A*, three peptides were synthesized containing the complete minimal DNA binding domain (Pwt) or mutated/truncated forms of this domain (Pmut and Pshort, respectively). Increasing amounts of each peptide were incubated with the probe described above, and protein-DNA complexes were analyzed by bandshift. *Panel C*, to define the DNA binding properties of Pwt, affinity coelectrophoresis was carried out. The 140-bp DNA probe used above was loaded into a wide slot of a 1% agarose gel. Upon migration the probe encounters perpendicularly placed lanes with increasing amounts of Pwt, which will retard the DNA. After electrophoresis the gels were dried and exposed.

binding to DNA is visible at ~300 nM (data not shown). Thus the efficiency of B2B10 binding is severalfold lower than that of B1B9, suggesting that it may contribute to some aspects of the

binding of the complete ZFP-37 linker, but it does not contain the core region. Shortening the B1B9 region further to the minimal histone H1 motif depicted in Fig. 1*B* results in the

B16B14-GST fusion protein that still binds DNA, albeit with less affinity than B1B9. Deletion of parts of the minimal histone H1 domain gives the B1B15-, B17B14-, and B18B14-GST fusion constructs and abolishes DNA binding completely (Fig. 4*A*). From these data we conclude that the histone H1-like domain in murine ZFP-37 binds DNA, but it may not be sufficient to reconstitute the complete DNA binding profile seen in KL1.

On the basis of the results with the GST fusion proteins three different peptides were synthesized: one covering the complete B16B14 DNA binding module (Pwt); a second peptide, mutated in 3 lysine residues that are highly conserved among the histone-like modules (Pmut); and a shorter peptide, covering part of the DNA binding motif (Pshort; see Fig. 4*B*). Bandshifts with these peptides showed that Pwt binding to DNA is visible at 10 μM, which is a 30-fold higher concentration than that required for B1B9 binding. Pmut and Pshort do not bind DNA, confirming that the core histone H1-like region cannot be shortened further and that the first 3 lysine residues of this domain are essential for DNA binding (Fig. 4*B*). Together the data demonstrate that the results obtained using the GST fusion proteins are not an artifact of the system, and hence these experiments identify a novel DNA binding domain in ZFP-37.

Affinity coelectrophoresis (19) was used to determine the affinity and cooperativity of Pwt binding to DNA (20), according to the model of McGhee and von Hippel (39). With this assay and using the 140-bp fragment as a probe (Fig. 4*C*), an intrinsic association constant (K) of 5×10^3 M^{-1} and a cooperativity factor (ω) of 8.5 were derived (20). These data suggest that Pwt binding to DNA is slightly cooperative. The association constant for singly contiguous sites, $K\omega$, is 4.5×10^4 M^{-1} ($K \times \omega$). Both K and ω are about 10-fold lower than the values calculated for another basic protein, clupeine Z (20), leading to a $K\omega$ that is 100-fold less. The proline repeat-containing segment from the bacterial replication arrest protein Tus, which somewhat resembles the ZFP-37 core linker domain (data not shown), also binds DNA with a much higher association constant, albeit in a noncooperative fashion (40). As noted above, the affinity of the complete ZFP-37 linker domain for DNA is likely to be much higher than that of Pwt because in bandshifts the concentration at which Pwt binding to DNA is detected is about 50-fold higher than that required for binding of KL1. Thus, the association constant for the complete linker domain could approach the K values of clupeine Z and Tus and, like Pwt, KL1 might bind DNA cooperatively.

In Vivo Isoforms of ZFP-37—Western blot studies suggested previously that proteins of 70 and 40 kDa, detected only in testis extracts, represent the *in vivo* isoforms of ZFP-37 (41). However, we have shown that the *Zfp-37* gene is also expressed in the brain and that it potentially encodes protein isoforms with or without a truncated KRAB-A region. These isoforms have a predicted molecular mass of ~67 or ~62 kDa, depending upon which ATG is utilized (13). To address these contradictory results, polyclonal antibodies either against the GST-ZFP-37 fusion proteins depicted in Fig. 2*A* or the Pwt peptide depicted in Fig. 4*B* were raised in rabbit and used to detect ZFP-37 on Western blots with nuclear protein extracts from various mouse tissues. Lysates of COS-1 cells, transfected with cDNAs encoding either a 67-kDa or a 62-kDa ZFP-37 isoform, or mock-transfected, were run along with the nuclear samples as control (Fig. 5*A*). In the COS-1 cells transfected with *Zfp-37*, proteins of 67 and 62 kDa are visualized which are not present in the mock-transfected cells (Fig. 5*A*, *left three lanes*). Thus, the antibodies detect the overexpressed proteins, and predicted molecular weights correlate well with the masses deduced after
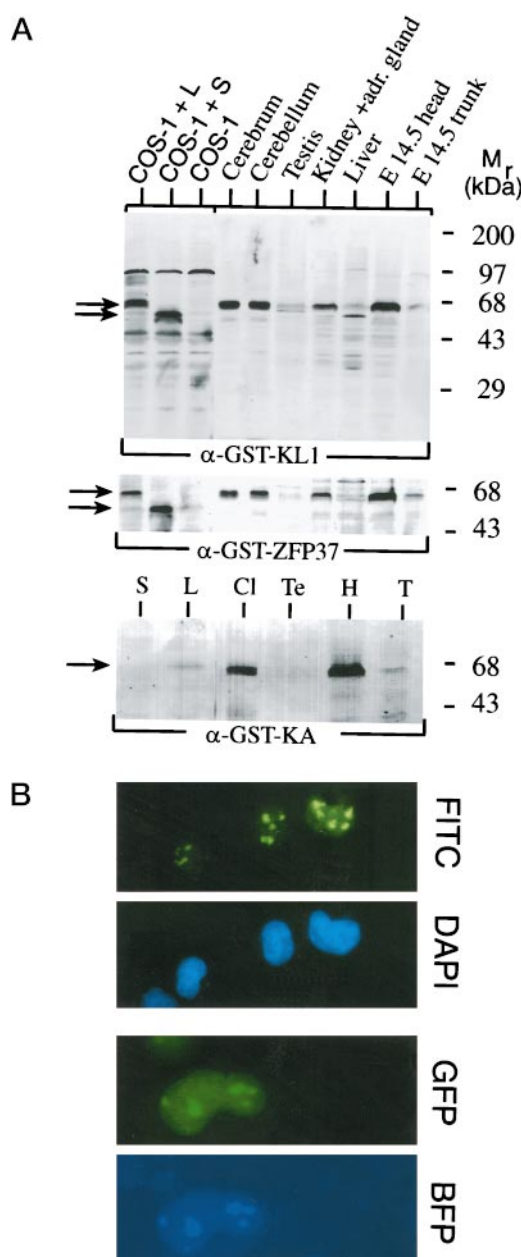

FIG. 5. **ZFP-37 isoforms in cells and tissues.** *Panel A*, COS-1 cells were transfected with cDNAs encoding the long (*L*) or short (*S*) isoform of ZFP-37, or they were mock transfected. 2 days later cells were harvested and total protein lysate made. Nuclear extracts of adult mouse tissues and embryonic day 14.5 head or trunk were run next to the COS-1 cell lysates on SDS-polyacrylamide gel electrophoresis. Western blots were incubated with antibodies against GST-KL1 (*upper panel*), full-length ZFP-37 (*α-GST-ZFP-37*; *middle panel*), or against GST-KA (*lower panel*). *Arrows* at the *left* indicate the position of the two isoforms of ZFP-37; molecular sizes of marker proteins are indicated at the *right*. *Cl*, cerebellum; *Te*, testis; *H*, E14.5 head; *T*, E14.5 trunk. *Panel B*, COS-1 cells, transfected with the 67-kDa ZFP-37 isoform, were fixed and incubated with α-GST-ZFP-37 antibodies followed by FITC-conjugated secondary antibodies. Nuclei were counterstained with DAPI. ZFP-37 localizes to aggregate structures in the nuclei, which resemble nucleoli. In the *lower panels*, COS-1 cells were cotransfected with plasmids encoding ZFP-37-GFP or NoLS-BFP. After 48 h cells were analyzed for colocalization of the two fusion proteins.

gel electrophoresis. Interestingly, several proteins of approximately the same size are detected within a single lane, indicating that ZFP-37 undergoes posttranslational modifications in COS-1 cells. A similar set of proteins, migrating at the position of the 67-kDa COS-1 cell-derived ZFP-37 isoforms, is detected in highly varying quantities in all of the tested nuclear

extracts (Fig. 5*A*, *upper* and *middle panels*). The fact that several antibodies against different ZFP-37 fusion proteins detect the same isoforms on Western blots suggests strongly that these 67-kDa proteins represent ZFP-37 *in vivo*. In contrast, the ~62-kDa liver protein, which is visible with the α-GST-KL1 antiserum (Fig. 5*A*, *upper panel*), is not detected with other antibody preparations (Fig. 5*A*, *middle panel*, and data not shown), and it is therefore not an isoform of ZFP-37. A third antiserum, directed against the KRAB-A domain of ZFP-37, recognizes only the long isoform in transfected COS-1 cells (Fig. 5*A*, *lower panel*), indicating that these antibodies are specific for the 67-kDa protein. A similar protein is also detected in cerebellar and embryonic tissue extracts with this antiserum, suggesting that in mice the main ZFP-37 isoforms contain the KRAB-A region.

To our surprise the tissue extracts containing most ZFP-37 are brain and kidney/adrenal gland, whereas in testis and liver only small quantities of the protein are visualized (Fig. 5*A*). The kidney/adrenal gland signal is due to the expression of *Zfp-37* in chromaffin cells of the adrenal medulla, a specialized nerve cell of the peripheral nervous system.[3] The lack of a strong protein signal in testis is in stark contrast to the mRNA expression profile, which shows that the *Zfp-37* message is most abundant in this tissue (13). We conclude that in testis little of the *Zfp-37* mRNA is translated, and/or testis-derived ZFP-37 has a very short half-life. The Western blot data are not consistent with those of another report (41), in which two ZFP-37 isoforms of 70 and 40 kDa are detected exclusively in testis. In that report no protein is visualized in brain extracts, and a 40-kDa form is detected in testis, indicating that the antibodies used are not monospecific.

Indirect immunofluorescense on transfected COS-1 cells was performed to assess the specificity of the anti-ZFP-37 antibodies and to localize overexpressed ZFP-37. This revealed that both the 67-kDa (Fig. 5*B*, *upper panel*) and 62-kDa (data not shown) ZFP-37 isoforms are localized in nuclear aggregates, although some fluorescence is also visible throughout the nucleus. These spots resemble nucleoli but might also represent heterochromatic domains and/or aggregates of overexpressed protein. Specific signals are seen only in transfected cells. Antibodies against the ZFP-37 KRAB-A region recognize the long isoform only (data not shown), in the same structures as seen in Fig. 5*B*. The suggestion that in transfected COS-1 cells ZFP-37 associates with nucleoli was tested in cotransfection experiments with ZFP-37-GFP and NoLS-BFP cDNAs. The first cDNA clone encodes a fusion protein of ZFP-37, linked to GFP (26). The second construct encodes a mutated form of GFP, called BFP (see "Experimental Procedures"), fused to a nucleolus targeting signal (NoLS; (29). The percentage of cells in which NoLS-BFP could be detected was low because of the low intensity of the fluorophore. However, in those cells expressing both NoLS-BFP and ZFP-37-GFP at a detectable level, colocalization of the two fluorescent tags is seen (Fig. 5*B*, *lower panels*). Together the results suggest that in dividing COS-1 cells ZFP-37 is targeted to nucleoli.

Intracellular Distribution of ZFP-37 in Vivo—The distribution of *Zfp-37* mRNA in embryonic and adult mice has been described previously (13). These data showed that in the developing mouse expression of *Zfp-37* is widespread, yet at 12.5 days postcoitus it is most intense in multipotent precursor cells of the nervous system. In adult mice *Zfp-37* mRNA expression is restricted to testis and brain, and in the latter tissue message is detected only in neurons. The same antibodies as used

in the COS-1 cell experiments were applied to ZFP-37 detection *in vivo* in adult mice. Because the Western blots established that most ZFP-37 expression occurs in brain, serial sections from this tissue were analyzed using wild type mice and a transgenic line overexpressing ZFP-37. A detailed description of how the transgenic line was derived will be presented elsewhere.[3] In all tissue sections, the antisera only gave specific signals when sections were microwave treated before antibody incubations (data not shown).

The immunocytochemistry in adult mouse brain reveals that ZFP-37 has a dynamic intracellular distribution pattern that might be dependent on neuronal cell type and/or metabolic activity. In Fig. 6, *panels a–c*, ZFP-37 expression in wild type mice is shown, and in *panels d–o*, the intracellular distribution of ZFP-37 in the transgenic mouse line is depicted. The antibody signal in the transgenic line is better because of the higher levels of protein, which indicates that in normal mouse brain not all binding sites for ZFP-37 are occupied. Similar distributions are seen with different anti-ZFP-37 antibodies (Fig. 6 and data not shown). In most neurons ZFP-37 is concentrated more at the periphery of the nucleolus than at the interior. This labeling pattern is, for example, observed in neurons from the entorhinal cortex (Fig. 6, *a–c*) and hippocampus (Fig. 6, *d–f*). It is quite obvious in hippocampal sections, analyzed with the use of a confocal microscope (*inset* in Fig. 6*e*). The most intense DAPI stain in these neurons is adjacent to, but does not colocalize with, the FITC label (compare Fig. 6, *panel a* with *panel c*). In many large neurons, on the other hand, the ZFP-37 signal is mainly adjacent to the nucleolus, clearly colocalizing with the intense DAPI stain; from there it extends into the nucleus in a speckled pattern. This type of labeling is, for example, detected in occulomotor neurons (Fig. 6, *g–l*). The only neurons where ZFP-37 consistently decorates the complete nucleolus are the Purkinje cells of the cerebellum (Fig. 6, *m* and *n*). To identify nucleoli within cell preparations we used phase-contrast microscopy in combination with epifluorescence. Because of their densely packed protein/RNA/DNA content nucleoli appear as dark spots within the context of the nucleus. The FITC label, representing ZFP-37 localization, overlaps with the very dense areas in the phase-contrast image (Fig. 6, *g, i, n, o*, and data not shown). In addition to the major patterns of ZFP-37 expression described above, antibody staining is also found occasionally throughout neuronal nuclei, in a speckled manner, for example, in the granule cell layer of the cerebellar flocculus (data not shown). Interestingly, the vast majority of granule cells of the cerebellum, which have minute nucleoli with an atypical organization (42), is among the neuronal cell types expressing little ZFP-37 (Fig. 6*m*). Together these data indicate that ZFP-37 associates with neuronal nucleoli, and the intraneuronal accumulation of ZFP-37 is related to nucleolar mass and/or structure.

Previous investigations have demonstrated that DAPI-positive spots, adjacent to neuronal nucleoli, represent centromeric DNA (43, 44). Given the frequent overlap between DAPI and ZFP-37 signals, this would imply that ZFP-37 contacts centromeric regions. Because we used microwave-treated sections to detect ZFP-37 expression patterns, it was essential to verify that the DAPI-positive perinucleolar stain in our experiments colocalized with centromeres. In the mouse, AT-rich repetitive satellite sequences, which are heavily methylated, constitute the majority of the centromere (45). As a consequence mouse centromeric DNA is covered by the methyl-CpG-binding protein MeCP2 (22). Antibodies against MeCP2 were therefore used to localize methylated centromeric DNA in the brain and to see if this signal overlapped with the DAPI stain. Like anti-ZFP-37 antisera, MeCP2 antibodies do not give a signal in

---

[3] D. Michalovich, T. Verkerk, F. Grosveld, and N. Galjart, unpublished observations.
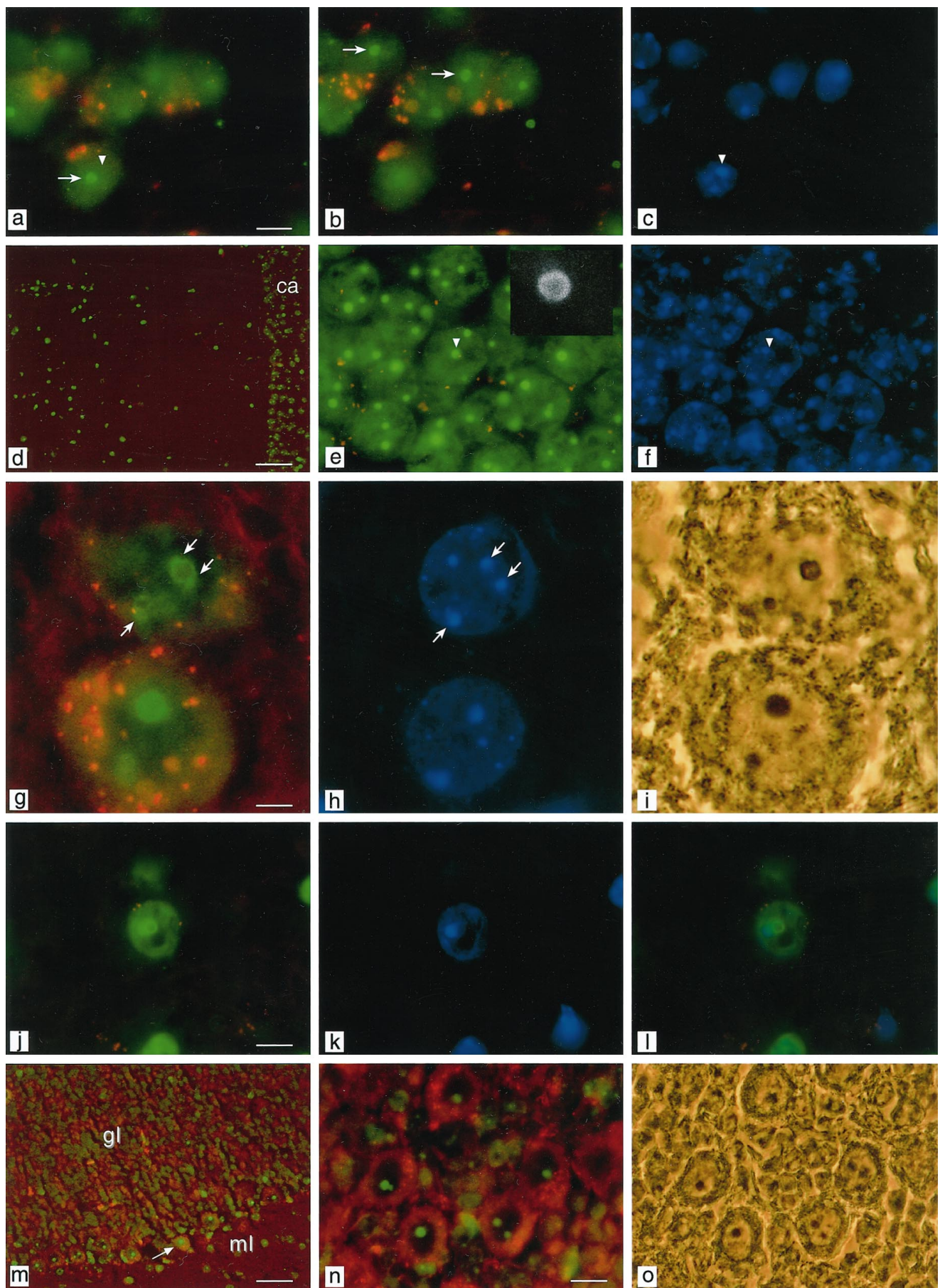
ZFP-37 May Define Neuronal Nuclear Domains

FIG. 6. **Intracellular distribution of ZFP-37 in adult CNS neurons.** Paraffin-embedded sections of 10 μm, derived from wild type (*panels a–c*) or transgenic (*d–o*) mice, were microwave treated and subsequently incubated with anti-ZFP-37 antibodies followed by FITC-conjugated
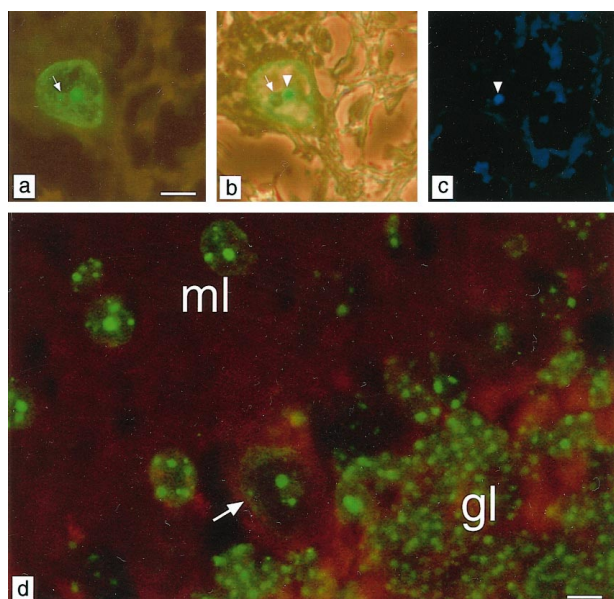
FIG. 7. **MeCP2 association with centromeric DNA.** Brain sections from wild type mice were treated as in Fig. 6 and incubated with a polyclonal antibody against MeCP2 followed by FITC-labeled secondary antibodies (*panels a*, *b*, and *d*). Sections were counterstained with DAPI (*c*). In *panels a–c* a brainstem neuron is shown, in which MeCP2 labeling mainly colocalizes with the DAPI-positive spot (*arrowhead* in *panels b* and *c*), which is adjacent to the nucleolus (*arrow* in *panels a* and *b*). The latter is identified by phase-contrast (*dark spot* in *panel b*). Thus, heavily methylated mouse centromeric DNA can be visualized with DAPI staining after treatment of sections with the microwave. Note that MeCP2 also labels the remainder of the perinucleolar region as well as heterochromatin attached to the nuclear membrane and that fine threads of the protein seem to emanate from the centromere into the cell nucleus. In *panel d* a section of the cerebellum is shown. Note the abundant speckled expression of MeCP2 in granule cells, which contain large amounts of heterochromatic DNA. Neurons in the molecular layer are also quite well stained; label in these basket and stellate cells is localized to two to six large dots, some of which could correspond to nucleolus-associated centromeric DNA. Purkinje cells (*arrow* in *panel d*) contain less MeCP2, which is mostly found capping the nucleolus. Scale bars: *a*, 5 μm; *d*, 4.3 μm.

neurons unless sections are microwave-treated (data not shown). This is despite the very high abundance of MeCP2 in brain (46). However, after antigen exposure, bright FITC signals are obtained throughout the brain (Fig. 7, *a–d*, and data not shown), which largely overlap with the DAPI-positive perinucleolar spots. The latter therefore represent centromeric DNA, and thus in neurons ZFP-37 frequently binds to centromeric DNA.

In the cerebellum MeCP2 labeling is abundant in granule cells and neurons of the molecular layer, whereas Purkinje cells are clearly less stained (Fig. 7*d*). Although less obvious than the centromeric staining, MeCP2 also decorates the perinucleolar rim (Fig. 7, *a* and *d*), similar to the ring structure of ZFP-37 found in motor neurons. Interestingly, with a few exceptions MeCP2 signals are always faint within nucleoli, even

though mouse rDNA repeats can be methylated (47, 48). This raises the possibility that a different methyl-CpG-binding protein binds to methylated rDNA in neurons or that methylated rDNA is recruited to the perinucleolar area, where it is bound by MeCP2.

Given the presence in ZFP-37 of a histone H1-like domain, staining of ZFP-37 in neurons was compared with that of histone H1, using antibodies that recognize all common H1 isoforms (23). Like ZFP-37, histone H1 was found to have a variable intracellular localization (data not shown). Purkinje cells of the cerebellum and pyramidal and granule cells of the hippocampus express little histone H1 while containing a clear ZFP-37 signal. We presume that in these cells histone H1 has been largely replaced by the differentiation-associated histone H1^0, a protein that is not recognized by the antibodies. Occasionally we do observe H1 labeling in Purkinje cells, which is at the rim of the nucleolus, similar to that found for ZFP-37 in motor neurons. Hence, the distribution of two architectural proteins, MeCP2 and histone H1, resembles that of ZFP-37 in that it is localized to specific chromatin domains in neuronal nuclei. In conclusion, ZFP-37 associates with constitutive heterochromatin surrounding the neuronal nucleolus, and/or it decorates the interior of the nucleolus. The distribution of ZFP-37 is dependent on the size, structure, and number of nucleoli, which in turn relate to the neuronal cell type and metabolic activity. Together with the *in vitro* results on ZFP-37-DNA interactions these data are compatible with a function for ZFP-37 as a protein involved in the formation and/or maintenance of specialized neuronal nucle(ol)ar chromatin domains.

DISCUSSION

In this report evidence is presented that the protein isoforms of murine ZFP-37 which occur *in vivo* are approximately 67 kDa and contain a truncated KRAB domain. ZFP-37 is detected mainly in the brain, where it is a nucleolar-associated protein that contacts heterochromatic regions of DNA. A novel DNA binding domain has been characterized in ZFP-37, which preferentially binds double-stranded DNA. In combination with previous mRNA *in situ* hybridizations (13), this suggests that in adult mice ZFP-37 is a specific constituent of neuronal nuclear chromatin.

Structure and Biochemical Function of ZFP-37—The amino acid sequence of ZFP-37 has three characteristic features. At the NH$_2$ terminus most ZFP-37 isoforms contain a truncated version of the KRAB domain. This region is followed by a basic linker domain, and at the COOH terminus all proteins have 12 zinc fingers of the C$_2$H$_2$ type. The KRAB domain has been defined as a 65-amino acid motif comprising two boxes, A and B, each predicted to form an amphiphatic helix (5). Recently, the KRAB domains from seven zinc finger proteins have been shown to act as potent transcriptional repressors when tethered to a heterologous DNA binding domain (7, 9, 10). The repressing activity was further mapped to conserved residues in the KRAB-A domain (7), the activity being dependent on DNA binding. We should note that some of the essential amino

secondary antibodies (*panels a*, *b*, *d*, *e*, *g*, *j*, *l*, *m*, *n*). Nuclei were counterstained with DAPI (*panels c*, *f*, *h*, *k*, and *l*), which labels mainly the repetitive DNA present in centromeres. The *red* signal is caused by autofluorescence. Phase-contrast pictures (*panels i* and *o*) allow the detection of nucleoli, which appear as densely stained spots. Note the accumulation of ZFP-37 at the outer edges of the nucleolus in neurons from the entorhinal cortex (*panels a* and *b*) and hippocampus (*panel e*). This accumulation is particularly clear after hippocampal nucleoli have been examined by confocal microscopy (*inset* in *panel e*). In *panels a–f* centromeric DNA is ZFP-37-negative (compare *arrowheads* in *panels a*, *c* (centromere), and *e*, *f* (nucleolus)). In *a* and *b*, different focal planes are shown, which brings different nucleoli into focus with the same localization of ZFP-37 (see *arrows* in *a* and *b*). In occulomotor neurons (*g–l*) ZFP-37 stains only the outer rim of the nucleolus (the *lower* cell in *g* is not in focus) and centromeric DNA (indicated by *arrows* in *g* and *h*). In *panel l* FITC and DAPI signals have been overlaid to demonstrate that ZFP-37 localizes to centromeric DNA. Cerebellar Purkinje cells show a more even distribution of ZFP-37 throughout the nucleolus (*m* is a low magnification, *n* is a high magnification). The *arrow* in *m* points to a Purkinje cell, which stains positively for ZFP-37. Note the colocalization of ZFP-37 with the darkest areas of the nucleoli in the phase-contrast pictures (compare *g* and *i*; *n* and *o*). *Ca*, pyramidal cells from the CA3 area of the hippocampus; *gl* and *ml*, granular and molecular cell layers of the cerebellum, respectively. Scale bars: *a*, 10 μm; *d*, 75 μm; *g*, 3.5 μm; *j*, 8.3 μm; *m*, 43 μm; and *n*, 6.3 μm.

acids are missing from ZFP-37, hence the presence of a transcriptional repressing activity in its KRAB domain remains to be ascertained. How the complete KRAB domain exerts its effect was unknown until the discovery that it associates with a corepressor, KAP-1 (49), TIF1b (50), or KRIP-1 (51). KAP-1/TIF1b/KRIP-1 is homologous to TIF1a (52), and like TIF1a, it has features that classify it among structural chromatin proteins. Scenarios where the very large family of KRAB-ZFPs represses transcription through KAP-1, or similar factors, have been proposed (49, 53). Interestingly, TIF1b can associate with mHP1 (53), a putative heterochromatin protein, linking the KRAB-ZFPs to inactive DNA. This fits with our finding that ZFP-37 localizes to constitutive neuronal heterochromatin. The observation that the KRAB-zinc finger gene *ZNF74* encodes an RNA- rather than a DNA-binding protein (54), together with the fact that the hnRNP K protein has been shown to associate with the KRAB-containing protein Zik-1 (55), indicates that other KRAB-zinc finger proteins may act in different pathways.

Although we failed to isolate a specific binding site(s) for the zinc finger domain of ZFP-37, we characterized a novel DNA binding domain in the basic linker stretch located between zinc finger and KRAB domains. This linker region binds double-stranded DNA preferentially. Stable (or rigid) complexes between ZFP-37 linker and DNA are detected at 250 nM fusion protein, which would correspond to approximately 30,000 molecules of ZFP-37/cell. For comparison, it has been reported that MeCP2 levels in the brain are roughly 6×10^6/nucleus (46). Therefore, the concentration at which ZFP-37 binds DNA *in vitro* could be physiologically relevant. Human ZFP-37 also contains the novel DNA binding domain, whereas the basic or cysteine-rich linker regions from five other KRAB-ZFPs do not. These data suggest that DNA binding by the linker domain of ZFP-37 is a conserved and relevant feature. The core DNA binding motif in human and mouse ZFP-37 resembles the COOH-terminal basic DNA binding regions of histone H1 and other proteins. Thus, as has been argued before (32), the correct placement of lysines and/or arginines in a framework of proline and alanine residues may create an efficient DNA binding motif. It is interesting to note that ZFP-37 is not the only nucleolar component with a histone H1-like DNA binding motif; nucleolin, no38, and the ribosomal protein L1 are also included in this family (see Fig. 1*B*).

Because histone H1 and ZFP-37 have partially overlapping DNA binding characteristics, it seems possible that ZFP-37 replaces histone H1 or one of its variants at specific chromosomal domains in neurons to obtain a further chromatin specialization. If true, this would place ZFP-37 in the group of histone H1 variants (56, 57). Interestingly, the histone H1-like domain of ZFP-37 resembles more the COOH termini of the replacement type histones H1^0 and H5 than those of the cell cycle-dependent histones. Like ZFP-37, histone H1^0 and H5 are present in terminally differentiated cell types (58), and it is thought that the higher content of basic amino acid residues in their tails reflects their capacity to condense DNA to a higher extent (59). Further research will have to determine how the linker region of ZFP-37 binds to DNA and to what extent this domain cooperates with the KRAB and zinc finger regions to yield a functional protein.

Intracellular Distribution and Function of ZFP-37—In the adult brain *Zfp-37* expression has been addressed previously by mRNA *in situ* hybridization (13). These data showed that *Zfp-37* is neuron-specific. Here we confirm the *in situ* data using antibodies against ZFP-37 and demonstrate that ZFP-37 isoforms are associated with constitutive heterochromatin adjacent to nucleoli and/or the interior of this compartment. This type of intracellular distribution has not yet been described for

other proteins. The data suggest that ZFP-37 plays a specific role in nucleolar/centromeric structure maintenance in neurons. This is in line with the fact that the nucleoli of most neurons have a different ultrastructure compared with nucleoli from other cell types (42–44, 60). In somatic cells, the pars granulosa (which is the main site for rRNA processing and ribosome formation) often surrounds the pars fibrosa (where the rDNA genes are transcribed), but in adult neurons these structures may be intertwined to form electron-dense nucleolonema that surround fibrillar centers. In addition, in neurons the centromeric region of many chromosomes can be found clustered on the nucleolus, indicating that the perinucleolar region is used as a centromere attachment site (43, 61, 62). It is noteworthy that granule cells of the cerebellum have a high amount of heterochromatin (43), yet they have poorly developed nucleoli, and consequently they lack the typical neuronal centromere/nucleolar phenotype (42, 43, 63). In most granule cells ZFP-37 expression is low. Thus, taken together these data suggest that the specific neuronal nucleolar/centromeric phenotype and the level of ZFP-37 expression are correlated.

The main functions of the nucleolus are rRNA synthesis, ribosome assembly, and ribosome storage (for review, see Ref. 64), although a role in the regulation of mRNA export from the nucleus to the cytoplasm has also been attributed to this subcompartment (65). The rDNA transcription rate is regulated as a function of cellular growth rate or cellular activity. As a consequence, nucleolar structure and volume may vary greatly among differently active and/or growing cells. Several studies have provided (indirect) links between neuronal activity and changes in nucleolar structure/volume (*e.g.* Ref. 66), centromeric DNA position (61), or expression level of structural gene products, such as H1^0 (67). Also, circadian-dependent changes in nucleolar volume and structure have been documented to occur in certain types of neuron in the rat (68). It appears from these studies that adaptive processes in the neuronal cytoplasm are accompanied by nuclear structural adaptations and *vice versa*. We hypothesize that ZFP-37 is involved in maintaining/changing neuronal nucleolar/centromeric architecture, and thereby it may regulate rRNA synthesis and ribosome assembly and/or storage. The essence of a neuronal protein like ZFP-37 is to bring about changes in nuclear structure, necessary for correct expression of genes, in an appropriate time frame.

REFERENCES

1. Pieler, T., and Bellefroid, E. (1994) *Mol. Biol. Rep.* **20,** 1–8
2. Bellefroid, E. J., Marine, J. C., Matera, A. G., Bourguignon, C., Desai, T., Healy, K. C., Bray-Ward, P., Martial, J. A., Ihle, J. N., and Ward, D. C. (1995) *Proc. Natl. Acad. Sci. U. S. A.* **92,** 10757–10761
3. Knochel, W., Poting, A., Koster, M., el Baradi, T., Nietfeld, W., Bouwmeester, T., and Pieler, T. (1989) *Proc. Natl. Acad. Sci. U. S. A.* **86,** 6097–6100
4. Klocke, B., Koster, M., Hille, S., Bouwmeester, T., Bohm, S., Pieler, T., and Knochel, W. (1994) *Biochim. Biophys. Acta* **1217,** 81–89
5. Bellefroid, E. J., Poncelet, D. A., Lecocq, P. J., Revelant, O., and Martial, J. A. (1991) *Proc. Natl. Acad. Sci. U. S. A.* **88,** 3608–3612
6. Crew, A. J., Clark, J., Fisher, C., Gill, S., Grimer, R., Chand, A., Shipley, J., Gusterson, B. A., and Cooper, C. S. (1995) *EMBO J.* **14,** 2333–2340
7. Margolin, J. F., Friedman, J. R., Meyer, W. K., Vissing, H., Thiesen, H. J., and Rauscher, F. J., III (1994) *Proc. Natl. Acad. Sci. U. S. A.* **91,** 4509–4513
8. Pengue, G., and Lania, L. (1996) *Proc. Natl. Acad. Sci. U. S. A.* **93,** 1015–1020
9. Pengue, G., Calabro, V., Bartoli, P. C., Pagliuca, A., and Lania, L. (1994) *Nucleic Acids Res.* **22,** 2908–2914
10. Witzgall, R., O'Leary, E., Leaf, A., Onaldi, D., and Bonventre, J. V. (1994) *Proc. Natl. Acad. Sci. U. S. A.* **91,** 4514–4518
11. Nelki, D., Dudley, K., Cunningham, P., and Akhavan, M. (1990) *Nucleic Acids Res.* **18,** 3655
12. Burke, P. S., and Wolgemuth, D. J. (1992) *Nucleic Acids Res.* **20,** 2827–2834
13. Mazarakis, N., Michalovich, D., Karis, A., Grosveld, F., and Galjart, N. (1996) *Genomics* **33,** 247–257
14. Saiki, R. K., Gelfand, D. H., Stoffel, S., Scharf, S. J., Higuchi, R., Horn, G. T.,

Mullis, K. B., and Erlich, H. A. (1988) *Science* **239,** 487–491

15. Smith, D. B., and Johnson, K. S. (1988) *Gene (Amst.)* **67,** 31–40
16. Sambrook, J., Fritsch, E. F., and Maniatis, T. (1989) *Molecular Cloning: A Laboratory Manual*, 2nd Ed., Cold Spring Harbor Laboratory, Cold Spring Harbor, NY
17. Feinberg, A. P., and Vogelstein, B. (1983) *Anal. Biochem.* **132,** 6–13
18. Sukegawa, J., and Blobel, G. (1993) *Cell* **72,** 29–38
19. Lim, W. A., Sauer, R. T., and Lander, A. D. (1991) *Methods Enzymol.* **208,** 196–210
20. Nedved, M. L., and Moe, G. R. (1995) *Anal. Biochem.* **227,** 80–84
21. Erickson, B. W., and Merrifield, R. B. (1976) in *The Proteins* (Neurath, H., and Hill, R. L., eds) 3rd Ed., pp. 255–527, Academic Press, New York
22. Nan, X., Tate, P., Li, E., and Bird, A. (1996) *Mol. Cell. Biol.* **16,** 414–421
23. Parseghian, M. H., Clark, R. F., Hauser, L. J., Dvorkin, N., Harris, D. A., and Hamkalo, B. A. (1993) *Chromosome Res.* **1,** 127–139
24. Lichtsteiner, S., Wuarin, J., and Schibler, U. (1987) *Cell* **51,** 963–973
25. Okayama, H., and Berg, P. (1983) *Mol. Cell. Biol.* **3,** 280–289
26. Chalfie, M., Tu, Y., Euskirchen, G., Ward, W. W., and Prasher, D. C. (1994) *Science* **263,** 802–805
27. Cubitt, A. B., Heim, R., Adams, S. R., Boyd, A. E., Gross, L. A., and Tsien, R. Y. (1995) *Trends Biochem. Sci.* **20,** 448–455
28. Heim, R., and Tsien, R. Y. (1996) *Curr. Biol.* **6,** 178–182
29. Schmidt, C., Lipsius, E., and Kruppa, J. (1995) *Mol. Biol. Cell* **6,** 1875–1885
30. Gluzman, Y. (1981) *Cell* **23,** 175–182
31. Galjart, N. J., Gillemans, N., Harris, A., van der Horst, G. T., Verheijen, F. W., Galjaard, H., and d'Azzo, A. (1988) *Cell* **54,** 755–764
32. Churchill, M. E., and Travers, A. A. (1991) *Trends Biochem. Sci.* **16,** 92–97
33. Pollock, R., and Treisman, R. (1990) *Nucleic Acids Res.* **18,** 6197–6204
34. Arranz, V., Harper, F., Florentin, Y., Puvion, E., Kress, M., and Ernoult-Lange, M. (1997) *Mol. Cell. Biol.* **17,** 2116–2126
35. Witzgall, R., O'Leary, E., Gessner, R., Ouellette, A. J., and Bonventre, J. V. (1993) *Mol. Cell. Biol.* **13,** 1933–1942
36. Pott, U., Thiesen, H.-J., Colello, R. J., and Schwab, M. E. (1995) *J. Neurochem.* **65,** 1955–1966
37. Perez, M., Rompato, G., Corbi, N., De, G. L., Dragani, T. A., and Passananti, C. (1996) *FEBS Lett.* **387,** 117–121
38. Lange, R., Christoph, A., Thiesen, H. J., Vopper, G., Johnson, K. R., Lemaire, L., Plomann, M., Cremer, H., Barthels, D., and Heinlein, U. A. (1995) *DNA Cell Biol.* **14,** 971–981
39. McGhee, J. D., and von Hippel, P. H. (1974) *J. Mol. Biol.* **86,** 469–489
40. Nedved, M. L., Gottlieb, P. A., and Moe, G. R. (1994) *Nucleic Acids Res.* **22,** 5024–5030
41. Hosseini, R., Marsh, P., Pizzey, J., Leonard, L., Ruddy, S., Bains, S., and Dudley, K. (1994) *J. Mol. Endocrinol.* **13,** 157–165
42. Lafarga, M., Berciano, M. T., Hervas, J. P., and Villegas, J. (1989) *J. Neurocytol.* **18,** 19–26
43. Manuelidis, L. (1984) *Proc. Natl. Acad. Sci. U. S. A.* **81,** 3123–3127
44. Manuelidis, L. (1984) *J. Neuropathol. Exp. Neurol.* **43,** 225–241
45. Miller, O. J., Schnedl, W., Allen, J., and Erlanger, B. F. (1974) *Nature* **251,** 636–637
46. Nan, X., Campoy, F. J., and Bird, A. (1997) *Cell* **88,** 471–481
47. Brock, G. J., and Bird, A. (1997) *Hum. Mol. Genet.* **6,** 451–456
48. Bird, A. P., Taggart, M. H., and Gehring, C. A. (1981) *J. Mol. Biol. J. Mol. Biol.* **152,** 1–17
49. Friedman, J. R., Fredericks, W. J., Jensen, D. E., Speicher, D. W., Huang, X.-P., Neilson, E. G., and Rauscher, F. J. III (1996) *Genes Dev.* **10,** 2067–2078
50. Moosmann, P., Georgiev, O., Le Douarin, B., Bourquin, J.-P., and Schaffner, W. (1996) *Nucleic Acids Res.* **24,** 4859–4867
51. Kim, S. S., Chen, Y. M., O'Leary, E., Witzgall, R., Vidal, M., and Bonventre, J. V. (1996) *Proc. Natl. Acad. Sci. U. S. A.* **93,** 15299–15304
52. LeDouarin, B., Zechel, C., Garnier, J. M., Lutz, Y., Tora, L., Pierrat, P., Heery, D., Gronemeyer, H., Chambon, P., and Losson, R. (1995) *EMBO J.* **14,** 2020–2033
53. Le Douarin, B., Nielsen, A. L., Garnier, J. M., Ichinose, H., Jeanmougin, F., Losson, R., and Chambon, P. (1996) *EMBO J.* **15,** 6701–6715
54. Grondin, B., Bazinet, M., and Aubry, M. (1996) *J. Biol. Chem.* **271,** 15458–15467
55. Denisenko, O. N., O'Neill, B., Ostrowski, J., Van Seuningen, I., and Bomsztyk, K. (1996) *J. Biol. Chem.* **271,** 27701–27706
56. Wolffe, A. P. (1995) *Curr. Biol.* **5,** 452–454
57. Wolffe, A. P., and Pruss, D. (1996) *Trends Genet.* **12,** 58–62
58. Khochbin, S., and Wolffe, A. P. (1994) *Eur. J. Biochem.* **225,** 501–510
59. Zlatanova, J., and Yaneva, J. (1991) *DNA Cell Biol.* **10,** 239–248
60. Peters, A., Palay, S. L., and Webster, H. deF. (1991) *The Fine Structure of the Nervous System: Neurons and Their Supporting Cells*, 3rd Ed., pp. 48–64, Oxford University Press, New York
61. Billia, F., Baskys, A., Carlen, P. L., and De Boni, U. (1992) *Brain Res. Mol. Brain Res.* **14,** 101–108
62. Manuelidis, L. (1991) *Proc. Natl. Acad. Sci. U. S. A.* **88,** 1049–1053
63. Brodsky, V. Y., Marshak, T. L., Karavanov, A. A., Zatsepina, O. V., Nosikov, V. V., Korochkin, L. I., and Braga, E. A. (1988) *Cell Differ.* **24,** 201–207
64. Schwarzacher, H. G., and Wachtler, F. (1993) *Anat. Embryol.* **188,** 515–536
65. Schneiter, R., Kadowaki, T., and Tartakoff, A. M. (1995) *Mol. Biol. Cell* **6,** 357–370
66. Lafarga, M., Berciano, M. T., Andres, M. A., and Testillano, P. S. (1994) *J. Neurocytol.* **23,** 500–513
67. Lafarga, M., Garcia-Segura, L. M., Rodriguez, J. R., and Suau, P. (1995) *Brain Res. Mol. Brain Res.* **29,** 317–324
68. Pebusque, M. J., Vio-Cigna, M., Aldebert, B., and Seite, R. (1985) *J. Cell Sci.* **74,** 65–74